ELSEVIER

Surface Science 412/413 (1998) 213–235

surface science

On the structure and evolution of the buried S/Au interface in self-assembled monolayers: X-ray standing wave results

P. Fenter [a,*], F. Schreiber [b], L. Berman [c], G. Scoles [d], P. Eisenberger [e], M.J. Bedzyk[a,f]

[a] *Argonne National Laboratory, Argonne, IL 60439, USA*
[b] *Max-Planck Institut für Metallforschung, 70569 Stuttgart, Germany*
[c] *National Synchrotron Light Source, Brookhaven National Laboratory, Upton, NY 11973, USA*
[d] *Princeton Materials Institute, Princeton University, Princeton, NJ 08542, USA*
[e] *Lamont-Doherty Earth Observatory, Columbia University, New York, NY 10027, USA*
[f] *Department of Material Science, Northwestern University, Evanston, IL 60208, USA*

Received 11 February 1998; accepted for publication 19 May 1998

Abstract

We describe a structural study of the S/Au interface for decanethiol monolayers (C10) on a Au(111) surface using the technique of X-ray standing waves (XSWs). The XSW results for full-coverage monolayers are inconsistent with any model incorporating a single sulfur adsorption site, such as the widely assumed threefold hollow site on the Au(111) surface. Instead, the XSW results reveal two distinct sulfur head group sites, each with a distinct lateral and vertical location with respect to the underlying gold lattice. We discuss structural models that are consistent with these results. We have also studied the evolution of the structure versus coverage with XSW and X-ray photoelectron spectroscopy (XPS) and have determined that the local S/Au interface structure of the "lying down" striped phase at low coverages (0.27 ML, 1 ML $= 4.62 \times 10^{14}$ molecules cm^{-2}) is indistinguishable from that of the "standing up" c(4×2) phase at saturation (1 ML). Some important implications concerning the structure and growth of these monolayers are discussed. © 1998 Published by Elsevier Science B.V. All rights reserved.

Keywords: Decanethiol; Gold; Metal–organic interfaces; Self-assembly; Single crystal surfaces; Surface structure, morphology, roughness, and topography; X-ray standing waves

1. Introduction

Self-assembled monolayers (SAMs) have attracted wide attention in recent years as a general technique for modifying the physical and chemical properties of a surface [1,2]. It is widely anticipated that the technique of self-assembly will be useful in controlling such diverse properties as adhesion, corrosion, and wettability [3,4].

The structure and growth of SAMs have been intensively studied with a wide range of techniques and for a number of different systems [5–18]. Yet, even for the most thoroughly studied SAMs, *n*-alkyl thiols [$CH_3(CH2)_{n-1}SH$, or Cn] on a Au(111) surface, little is directly known about the bonding between the sulfur head group and the Au(111) substrate, and important fundamental structural issues remain either unresolved or controversial. The structure of the Cn/Au(111) system

* Corresponding author. Present address: Argonne National Laboratory Environmental Research Division, Bldg 203, 9700 South Cass Avenue, Argonne, IL 60439, USA.

PII: S0039-6028(98)00428-2

is often described as a hexagonal $\sqrt{3}\times\sqrt{3}R30^\circ$ lattice of thiol molecules, and it is widely assumed that the sulfur head groups form a hexagonal lattice and occupy the threefold hollow sites of the Au(111) surface (we refer to this as the "standard" model) [1,6,19–22]. This assumption has been supported by quantum chemical calculations [23] and is consistent with the observation that elemental sulfur is widely observed to adsorb in "highly coordinated sites" on transition metal surfaces [24], such as the threefold hollow site on of face-centered cubic f.c.c.(111) surfaces and hexagonally closed packed h.c.p.(0001) surfaces {e.g. S/Ni(111) [25] and S/Ru(0001) [26], respectively} or the fourfold hollow sites on f.c.c.(001) surfaces {e.g. S/Cu(001) [27,28]}.

However, this picture has yet to be experimentally demonstrated for the Cn/Au(111) system. Although early electron and He atom diffraction studies observed a $\sqrt{3}\times\sqrt{3}R30^\circ$ diffraction pattern for this system [12,29], these observations have no bearing on the lateral head group position, which cannot be determined from the diffraction pattern symmetry. Instead, the head group position can only be determined through an intensity analysis, which was not performed. Similarly, although scanning probe microscopy (SPM) provides molecular-level images of the monolayer [5–7,30], these results have yet to provide any information concerning the head-group location with respect to the underlying substrate lattice since it is not apparent, a priori, how the detailed features in the SPM images are correlated to the molecular-level structure, or even which component(s) of the monolayer (e.g. hydrocarbon chain, sulfur head group, Au substrate displacements) contribute to the SPM images. In other words, in spite of their value for many other issues, SPM techniques and diffraction pattern symmetries do not provide any direct evidence concerning the sulfur head group adsorption structure.

In fact, the equilibrium unit mesh of Cn/Au(111) is known {from X-ray [9,10,31] and He atom diffraction [11], as well as scanning tunneling microscopy (STM) [6,7]} to be in the form of the so-called $c(4\times2)$ superlattice of the $\sqrt{3}\times\sqrt{3}R30^\circ$ lattice (shown in Fig. 1), which is a

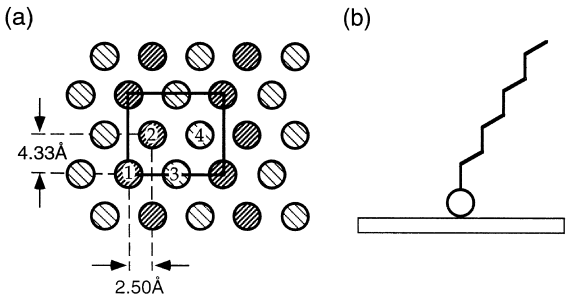

Fig. 1. (a) Schematic of the symmetry of the $c(4\times2)$ phase, in which each molecule is schematically drawn as a filled circles, and the two types of shading denote molecules that are distinct within the $c(4\times2)$ unit mesh (shown as a rectangle). For reference to the text, the molecules are numbered such that molecules 1 and 2 are equivalent, but are distinct from the molecules 3 and 4. (b) A schematic of an adsorbed thiol, showing the sulfur head group (circle) and the hydrocarbon chain (zigzag line).

rectangular unit mesh containing four molecules. From the symmetry of the diffraction pattern (which is revealed through the absence of certain Bragg peaks), it is directly known that molecule 2 is equivalent to molecule 1, and is displaced by an amount of $(x_2–x_1,\ y_2–y_1)=(2.50\ \text{Å},\ 4.33\ \text{Å})$ as shown schematically in Fig. 1 (and similarly for molecules 3 and 4), so that only two of the four molecules in the unit mesh are distinct [9,10]. Multiple "variants" of the $c(4\times2)$ unit mesh have been proposed on the basis of the STM data [6]. Of these variants, only that shown in Fig. 1 is consistent with the observed symmetry of the X-ray diffraction patterns [9,10], which suggests that the other variants are either non-equilibrium structures or artifacts of the STM measurement. While the $c(4\times2)$ symmetry does not reveal either the relative spacing between molecules 1 and 3 or their individual adsorption site(s), it does demonstrate unambiguously that molecules 1 and 3 (and similarly for molecules 2 and 4) in Fig. 1 are structurally distinct; if they were not distinct, then the extra diffraction peaks associated with the $c(4\times2)$ unit mesh would not be observed, resulting in a simple $\sqrt{3}\times\sqrt{3}R30^\circ$ unit mesh. Consequently, the $c(4\times2)$ symmetry can be thought of as a symmetry breaking of the $\sqrt{3}\times\sqrt{3}R30^\circ$ unit mesh that distinguishes molecule 1 from molecule 3. Because the symmetry applies to the monolayer as a whole, it will be reflected in the structure of all

components of the molecule (including the lateral and vertical head group position, and the lateral spacings and twist angles of the hydrocarbon chain). Consequently, the observed $c(4\times2)$ symmetry dictates that the head group position for these two molecules must be different at some level of precision. The questions that remain are then as follows:

(1) Is the head group structure revealed as small displacements (of a few hundredths of an Ångstom) about a single head group site, or do two clearly distinct head group locations exist?

(2) What are the exact head group locations?

The aim of this paper is to address the question of the location(s) of the sulfur head groups on the basis of the X-ray standing wave data.

The symmetry of the $c(4\times2)$ unit mesh can, in principle, support a wide range of head group structures. For instance, an X-ray crystallographic analysis of this system has determined [9] that the monolayer structure consists of a nearly hexagonal array of hydrocarbon chains (having a spacing of ~5 Å) but with a pairing of the sulfur head groups, resulting in a lateral S–S spacing of 2.2 Å. Due to the similarity between this derived S–S spacing and that found for disulfide compounds ($d_{S\text{–}S}=2.0$ Å) [32], this result was interpreted in the context of a disulfide adsorption state. For generality, we refer to this model as the "sulfur-pairing model". This model directly implies that two inequivalent sulfur binding sites exist in this system. Although this result was unexpected, it was nevertheless consistent with all known experimental date of the Cn/Au(111) system. Optical sum frequency generation (SFG) studies have further supported the sulfur-pairing model by independently showing that the symmetry of the monolayer is inconsistent with a $\sqrt{3}\times\sqrt{3}R30^\circ$ hexagonal array [14].

In contrast, recent theoretical work largely supports the "standard" structural model for this system, albeit with some ambiguity. For instance, recent calculations in which the surface is represented by a cluster of atoms confirm a preference of the sulfur head group for the f.c.c. threefold hollow site [33]. Furthermore, energy minimization calculations [34] found 22 structures that differed from the lowest energy structure by less than 1 kcal mol^{-1}, but were unable to reproduce the experimentally observed $c(4\times2)$ structure as the lowest energy structure, suggesting that a critical element of this system is still missing. Instead, structures consisting of smaller unit meshes were consistently found to have the lowest energy. However, of the 11 lowest energy four-chain structures, only one is consistent with the experimentally observed equilibrium symmetry of the $c(4\times2)$ unit mesh as shown in Fig. 1; all others can be ruled out based on symmetry considerations alone. Similarly, recent molecular dynamics (MD) simulations have been used to elucidate the structure of the $c(4\times2)$ superlattice, and concluded that "there may be several structures which correspond to the $c(4\times2)$ superlattice" [35]. Yet, here too there are clear discrepancies with the experimental results. For the structures that were found to be stable, the hydrocarbon tilt direction was inconsistent with that measured by GIXD [10,36]. Furthermore, the sulfur head-group arrangement for each of these structures could be characterized by a hexagonal $\sqrt{3}\times\sqrt{3}R30^\circ$ lattice with only minimal displacements, in disagreement with the GIXD intensity analysis [9]. Finally, these MD simulations predict [37] continuous changes in the monolayer structure at temperatures between 40 and 300 K that are not observed experimentally [10,31,38].

A common thread to all of these theoretical studies has been the a priori assumption that the S/Au interaction can be described without any explicit interaction between the sulfur head groups that might result in S–S pairing. Consequently, if a S–S interaction were to be an important element of the structure (as suggested by the GIXD results), then there is no reason to expect any meaningful agreement between these experimental and theoretical results. The only exception is a study by Gerdy and Goddard et al. [39] that explicitly assumed the presence of an S–S bond, in which their MD results were found to be in quantitative agreement with the GIXD scattering intensities.

A large gap clearly remains between the widely accepted "standard" bonding model (in which the

sulfur head group binds uniquely in a threefold hollow site) that is supported primarily by theoretical work, and the proposed "sulfur-pairing" model (which directly implies the existence of two distinct sulfur binding sites and the possibility of a S–S bond) based upon the GIXD results. This situation motivates the need to apply additional structural tools to this system that are based upon the direct relationship between molecular structure and experimental observables that is quantitatively established by fundamental physical laws (e.g. Maxwell's equations for X-ray scattering techniques). These techniques therefore can place important constraints upon the structure independent of any assumptions about the system, and in many cases, the structure can be directly determined. Most importantly, since these techniques are truly quantitative, it is possible to directly compare the experimentally derived structure with the results of the suitably precise theoretical treatment to independently test the level of our understanding.

While the nature of the S/Au interaction remains controversial, it is the ability of this system to "self-assemble" at room temperature that is clearly the most important and interesting characteristic of these SAM systems, and undoubtedly depends on the ability of individual molecules to diffuse across surface terraces to achieve highly ordered layers. However, any fundamental understanding of the growth behaviour must be ultimately based on a better understanding of the nature of the S/Au bond, since the equilibrium structure and the diffusion barrier are likely to be closely related (since the former is determined only by the position of the minimum in the multiparameter free energy surface that describes the structure of this system, and the latter is determined by the shape of the free energy surface away from the minimum). Ultimately, these issues can be resolved through a theoretical determination of the diffusional barriers, but these quantities can be meaningfully calculated only when the most fundamental quantity, the equilibrium geometric structure, has been firmly established.

Given the gap in our understanding between recent experimental and theoretical studies of the S/Au head group structure, and given the importance of the head group structure towards our understanding of the "self-assembly" process, further work is clearly warranted to elucidate the sulfur head group structure. At the least, such a broad discrepancy suggests that the critical features of the Cn/Au(111) system remain to be understood. By further elucidating the complexities of the sulfur head-group structure, we may also have the opportunity to advance our understanding of chemical bonding at metallic interfaces in general. The need for a firmer basis for understanding the influence of chemisorption on molecular bonds has been made dramatically clear in a recent paper by Nilsson et al. [40], in which the commonly accepted bonding models for CO and N_2 on transition metal surfaces have been found to be in need of revision.

The outline of this paper is as follows: In Section 2, we describe the principles of the XSW technique, and in Section 3, we discuss the experimental details specific to this experiment. Given the controversy related to the structure of this system, and given the relatively few studies of similar systems with XSW, we separate for clarity the description of the experimental data and the information that can be derived directly from them (Section 4) from the discussion of the specific head group locations (Section 5). We then discuss the interpretation of the data and the synthesis of models consistent with the data (Section 6), and our conclusions (Section 7).

2. The X-ray standing wave technique

There are very few quantitative techniques that can probe the buried S/Au interface structure. Although a broad range of techniques exist (e.g. electron-based techniques, such as low-energy electron diffraction) that are very powerful probes of adsorbate structures (e.g. elemental sulfur on a metal surface), the presence of a $\sim$15 Å-thick hydrocarbon layer presents a formidable barrier to most of these techniques due to the small inelastic mean free path of low-energy electrons [41]. Therefore, we have applied the XSW technique to probe in a quantitative and direct way of the S/Au(111) interface structure of the

C10/Au(111) SAM, and to elucidate further the nature of the organometallic bonds in this system.

The XSW technique is a precise, element-specific, structural probe that can determine the location of a particular species (in this case, sulfur) at surfaces [42,43], at buried interfaces [44], within Langmuir–Blodgett multilayer structures [45,46], as a bulk lattice impurity [47], and very recently within self-assembled monolayers [48]. Because XSW can, in favourable cases, provide atomic locations with an uncertainty of <0.02 Å, it has the ability to provide bond lengths at a precision sufficient to reveal chemical formation.

The XSW field is an interference pattern created by the coherent sum of an incident and reflected X-ray beam and is typically created by using a strong substrate Bragg reflection condition [notated as H to signify an arbitrary Bragg reflection (hkl)] and shown schematically in Fig. 2a. Because the phase (i.e. position in space) of the XSW field changes as the substrate crystal is scanned through the diffraction condition, the net result is a modulation in the X-ray absorbtion signal, Y, as the XSW anti-node passes through the atomic position of interest. This can be described formally as [42]

$$Y(E\gamma)/Y_0 = 1 + R(E\gamma) + 2f_H[R(E\gamma)]^{1/2} \times \cos[v(E\gamma) - 2\pi P_H] \quad (1)$$

where $R(E\gamma)$ is the substrate reflectivity as a function of the photon energy, $E\gamma$, and is given by $R(E\gamma) = [\mathscr{E}_H(E\gamma)/\mathscr{E}_0(E\gamma)]^2$ (for reasons discussed below, in this experiment, we vary the diffraction condition through $E\gamma$); $\mathscr{E}_0$ and $\mathscr{E}_H$ are the incident and diffracted beam electric field amplitudes; $v(E\gamma)$ is the energy-dependent phase of $\mathscr{E}_H$ relative to $\mathscr{E}_0$; Y_0 is the X-ray absorption signal away from the Bragg reflection condition; and f_H and P_H are, respectively, the "coherent fraction" and "coherent position" whose meaning and significance are discussed further below. Consequently, an XSW measurement entails monitoring the X-ray absorption through, for instance, the photoelectron yield or the X-ray fluorescence corresponding to a particular element (e.g. sulfur) as a function of the photon energy as the latter is scanned through the substrate Bragg condition.

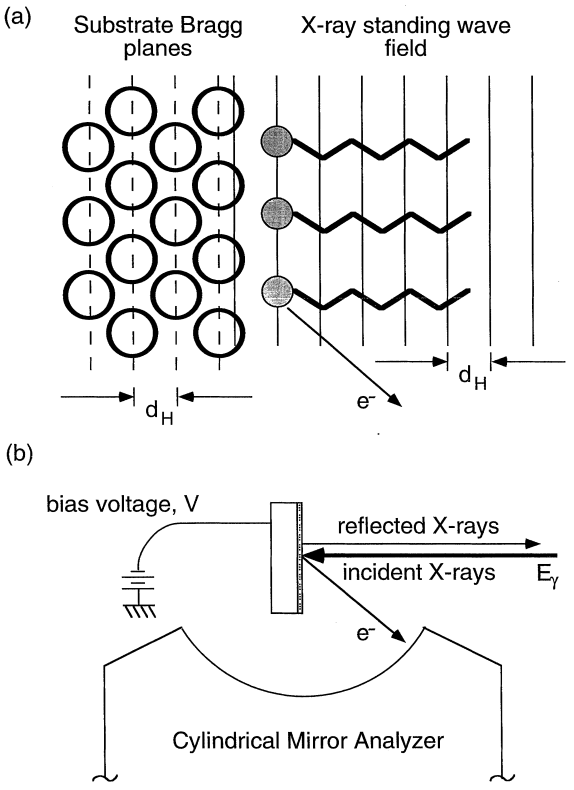

Fig. 2. (a) XSW measurement is shown in a microscopic perspective; the open circles denote the substrate lattice atoms, the filled circles denote the sulfur head group, and the zigzag line denotes the hydrocarbon chain. The vertical dashed lines indicate the Bragg plane spacing, d_H, used to create the XSW field (indicated by the solid vertical lines). As drawn, the head group position corresponds to the antinode of the XSW field. (b) A schematic of the XSW equipment is shown in which the incident and reflected X-ray beams are normal to a substrate surface, and the photoelectron, e^-, is detected with a single pass CMA whose axis is perpendicular to the incident beam direction.

Since the X-ray scattering and absorption processes are quantitatively understood, the structure can be determined through a direct comparison of experimental data and theoretical calculations (based on the full dynamical theory of X-ray diffraction [49]). For each XSW measurement at a particular diffraction condition, H, the coherent position, P_H, and the coherent fraction, f_H, are determined by a chi-squared fit of Eq. (1) to the XSW induced modulation of the characteristic emission signal from the adsorbate atom. Because P_H and f_H are the only quantities in Eq. (1) that

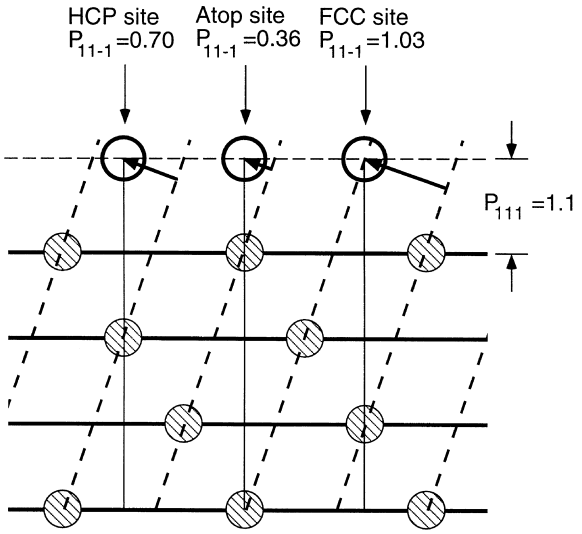

Fig. 3. Relationship between the coherent position and the adatom adsorption site is shown for the h.c.p., atop, and the f.c.c. adsorption sites on an f.c.c.(111) surface. The filled circles denote the f.c.c. substrate lattice, and the horizontal solid lines and dashed lines show the (111) and (11-1) Bragg planes, respectively. The vertical solid lines denote three adsorption site, the atop, h.c.p. and f.c.c. sites, which are found directly above the first-, second- and third-layer substrate atoms, respectively. In each case, the height above the surface is fixed at a height of $z=2.59$ Å, corresponding to a coherent position of $P_{111}=1.1=z/d_{111}$. Each of these adsorption sites is readily distinguished by its (11-1) coherent position, which is 0.36, 0.70 and 1.03, for the atop, h.c.p. and f.c.c. sites, respectively.

are not known a priori, each set of XSW data is fully characterized by these two parameters, which represent the normalized phase and amplitude of the Hth Fourier component of the adatom distribution, respectively.

Since each XSW measurement provides a one-dimensional measure of the structure, the full three-dimensional structure is revealed by performing XSW measurements using multiple substrate Bragg conditions, H. This is illustrated in Fig. 3 for three different lateral sites: the "atop" site, and the "f.c.c." and "h.c.p." threefold hollow sites.

For an adatom that occupies n different sites within the unit cell, and has m different symmetry equivalent orientations with respect to the substrate lattice, the superposition principle can be applied to describe this Hth Fourier component of the adatom distribution, F_{obs}:

$$F_{\mathrm{obs}} = f_H \exp(i2\pi P_H) = (1/N)\sum_l \left[\sum_j g_j D_{Hj} \exp(i2\pi \Delta_{j,l}/d_H) \right], \quad (2)$$

where g_j is the occupation factor for the jth site Δ_{jl} is the position of the jth site relative to the Hth diffraction planes, and D_{Hj} is the Debye–Waller factor of the adatom in the jth site. Consequently, the coherent position is directly related to the coherently averaged position of sulfur atoms, and the coherent fraction is sensitive to the distribution of sulfur about the average position. Since P_H is periodic with period d_H, as shown in Fig. 2a, the coherent position has a modulo-d ambiguity (i.e. $P=0.2$ is the indistinguishable from $P=1.2$). The coherent fraction, by definition is equal to unity, $f_H=1$, for atoms located in a unique high-symmetry adsorption site, and $f_H<1$ for atoms that occupy a distribution of sites (through either vibrations, static disorder, or multiple inequivalent adsorption sites).

For non-ideal systems, multiple contributions to the coherent fraction will exist that must be disentangled so that their structural implications can be properly interpreted. The experimentally measured coherent fraction, f_H, at a particular Bragg condition, H, can be written [42] as the product of the fraction of ordered molecules, C, a Debye–Waller factor to account for thermal vibrations, D_H, and the geometrical factor, a_H, which contains the structural information, or:

$$f_H = CD_H a_H. \quad (3)$$

Let us discuss each of these terms separately.

(1) If a fraction of molecules, C, are in well-defined sites and the remaining molecules are arranged randomly, the measured coherent fraction will reflect only the ordered fraction of molecules, as might be encountered as a result of adsorption at substrate lattice inhomogeneities instead of well-defined terrace sites.

(2) For any finite ad-atom vibrational amplitude, u, the coherent fraction will be reduced by a

Debye–Waller factor:

$$D_H = \exp[-(2\pi u/d_H)^2/2]. \quad (4)$$

This factor will be sensitive also to the substrate temperature through thermally induced changes in the vibrational amplitude of the adatom, $u(T)$. While adatom vibrational amplitudes are typically observed to be isotropic at room temperature, this need not be the case. In this case, the XSW technique is sensitive to the projection of the three-dimensional vibrational ellipsoid along the direction of measurement, H, resulting in $u = u_H$.

(3) Structural contributions to the coherent fraction through a_H include both (i) low-symmetry adsorption sites and (ii) multiple adsorption sites. A low symmetry adsorption site may reduce the coherent fraction because the observed coherent fraction is symmetry-averaged over all equivalent sites. For instance, an adatom in a low-symmetry site on a (111) surface having a unique vertical hight above the surface (and therefore $a_{111} = 1$) will have a reduced geometrical factor for measurements in off-normal directions. To illustrate this explicitly, we take the example of an XSW measurement of an adatom in a bridge site of an f.c.c.(111) surface, using the (11-1) substrate Bragg peak (which is tilted from the surface normal by an angle of 70.53°). The bridge site has a geometrical factor of $a_{11\text{-}1} = 1/3$, regardless of the height of the atom, z, above the surface. Qualitatively, this can be described as due to the out-of-phase contributions from two of the three bridge sites resulting in a geometrical factor of $a_{11\text{-}1}(1\text{-}1+1)/3 = 1/3$. For completeness, we note that in this case, the coherent position provides an additional independent measurement of the adatom height through the relation, $P_{11\text{-}1} = 0.5 + 0.1415z$. Multiple adsorption sites will also reduce the geometrical factor in a similar fashion. In the case of two distinct adatom sites, the measured coherent position will reflect the coherently averaged adatom position, and the geometrical factor will vary as $a_H \sim \cos(2\pi\delta/d_H)$, where δ is the deviation of each sulfur atom from the average position projected along the diffraction condition, H. Consequently, for an adatom layer that is buckled vertically by δ (but with an average height, z), an XSW measurement will reveal the average height through the coherent position and the buckling amplitude through the coherent fraction. In a similar way, the coherent fraction and position for any arbitrary structure can be calculated simply by using Eq. (2). Since the measured coherent fractions may contain contributions from all three terms in Eq. (3), these contributions must be explicitly addressed to derive uniquely the adatom location(s) derived from the geometric factor a_H.

3. Experimental

3.1. XSW and X-ray photoelectron spectroscopy

The XSW measurements were performed in the back-reflection geometry [43] (i.e. with scattering angle of 180°) as shown schematically in Fig. 2b. In this geometry, the momentum transfer is determined by the photon energy, $E\gamma$, so that Bragg's law can be written as $Q = 4\pi E_\gamma/hc = 2\pi/d_H$ (where h is Planck's constant, c is the speed of light, and d_H is the Bragg plane spacing), and the momentum transfer is determined by the photon energy. Consequently, the (111) Bragg peak of Au, having a bragg spacing, $d_{111} = 2.355$ Å, corresponds to a photon energy of $E_\gamma = hc/2d = 2632$ eV. The back reflection geometry is widely used in XSW measurements of metal substrates because it has the advantage that the measurements become insensitive to mosaic disorder typically found in metal "single-crystal" substrates because the Darwin width predicted by the dynamical theory of X-ray scattering becomes large ($\sim 1°$) for low-index Bragg reflections [43]. For example, in the back-reflection condition, the Au(111) reflection has a Darwin width of 2° (if measured in angle space) or equivalently 1.9 eV (in energy space). For comparison, the mosaic width of the crystal used in this study was independently measured to be $\sim 0.02°$. The measurements reported below were performed at the X24A beamline at the National

Synchrotron Light Source, which is optimized to deliver a high flux at soft X-ray energies through the use of a windowless beamline design. A monochromatic X-ray beam was obtained from the broad-band X-ray synchrotron beam by the use of a Si(111) double-crystal monochromator and was focused on to the sample by using a toroidal focusing mirror [50].

The local electric field of the XSW produced by the Bragg reflection is probed with S–K(1s) and Au–$M_V(3d_{5/2})$ photoelectron peaks, which have binding energies of 2472 and 2206 eV, respectively. The photoelectron spectrum is measured by using a single-pass cylindrical mirror analyzer (CMA) located at 90° to the X-ray beam direction with the CMA axis parallel to the X-ray polarization direction. Typical photoelectron spectra of the Au–$M_V(3d_{5/2})$ and the S–K(1s) photoelectron peaks are shown for a saturated C10/Au(111) monolayer ($\Theta=1$) in Fig. 4. A photon energy of $E\gamma=3136$ eV was used for XPS measurements. In all measurements, the photoelectron signal reported is measured by subtracting the background intensity (determined by extrapolating the background signal from measurements at higher electron kinetic energy) from the peak intensity. For the XSW measurements, the photoelectron signal is measured as a function of the photon energy (as it is scanned through the Bragg peak) by simultaneously scanning the CMA pass energy to compensate for changes in the photoelectron kinetic energy due to the changing photon energy.

We have looked carefully for any changes in the sample that might be associated with the X-ray exposure. We have not observed any spectroscopic changes in the position, width, or intensity of the sulfur photoelectron spectra as a function of X-ray dose; nor have we observed any systematic changes in the S or Au XSW spectra for successive measurements. Although the X-ray photoelectron spectroscopy (XPS) data are sensitive to the chemical state of the sulfur (e.g. thiol vs. thiolate), the XSW spectra provide an extremely sensitive measure of the geometrical structure (to within ± 0.02 Å). Since we have observed no evidence for damage due to X-ray exposure under our experimental conditions, we therefore conclude that the present results are intrinsic to the C10/Au(111) system.

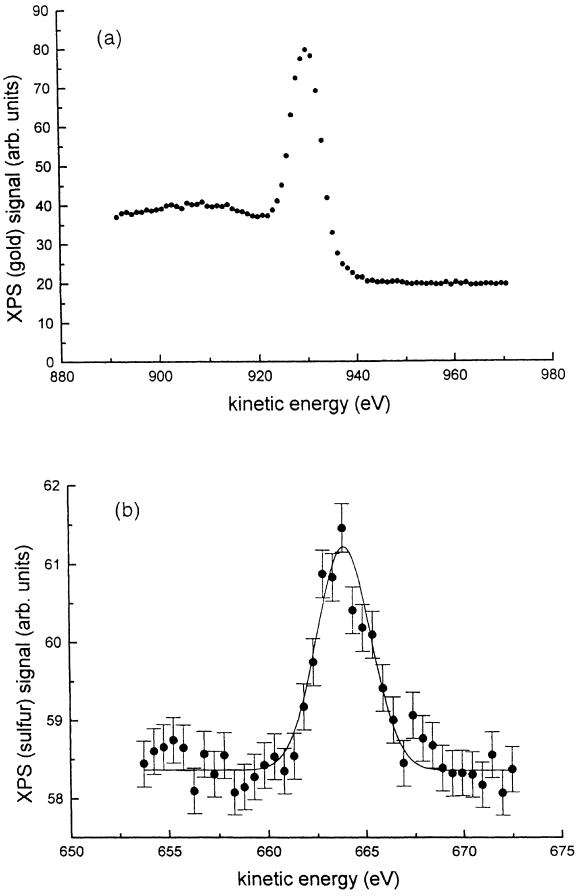

Fig. 4. Photoelectron spectrum for a saturated monolayer of C10/Au(111) showing (a) Au-$3d_{5/2}$ and (b) S-1s photoelectron yields. The data are plotted as a function of the electron kinetic energy for an incident photon energy of $E\gamma=3136$ eV. Statistical error bars are not shown for the Au-$3d_{5/2}$ data because the error bars are too small to be visible.

Reports of the X-ray-induced damage of SAMs in the synchrotron X-ray beam vary greatly. For simplicity, we compare results using GIXD studies at room temperature using focused monochromatic bending magnet sources at the NSLS, having a typical photon flux of 10^9-10^{10} photons s^{-1} and a photon energy of $\sim$8–10 keV. Damage is typically observed in the form of an exponential loss of scattering intensity, which can be characterized by a "damage time constant", τ_d. For siloxane monolayers on silicon substrates in a He atmosphere [51], $\tau_d \sim 90$ min. In contrast, the rate of X-ray-induced damage is typically significant

slower for thiol monolayers on Au(111). For instance, $\tau_d \sim 1.1 \times 10^4$ min for complete monolayers at ultra-high vacuum (UHV) conditions [31], as compared to $\tau_d \sim 1.2 \times 10^3$ min in an atmosphere of helium (A. Eberhardt et al., unpublished data), and $\tau_d \sim$ "a few hours" under an aqueous solution [52]. Whereas this diverse behaviour is undoubtedly related to a range of parameters including the substrate electronic structure and the photon energy [53] (which influence the photoelectron yield and kinetic energy, respectively), the dependence of τ_d upon the sample environment for Cn/Au(111) clearly demonstrates that it is closely related to the availability of reactive species from the sample environment. Because the present measurements are performed under UHV conditions, the lack of any significant X-ray induced damage in the XSW studies is, therefore, not surprising. Recent XPS results [54] have demonstrated a dramatic X-ray-induced change in the XPS spectra, but at both, a significantly ($>100\times$) higher photon dose than in the GIXD experiments [31], and a significantly lower (i.e. more damaging) photon energy.

3.2. Sample preparation

As we are interested in the behaviour that is intrinsic to the C10/Au(111) system, we have taken great care to produce very high-quality, clean, and well-ordered Au(111) single crystalline surfaces for use as the SAM substrate. In contrast, most studies of SAMs are performed using lower-quality evaporated Au films. Since factors such as surface roughness, the presence of steps and other defects, as well as possible contamination of the substrate surface when transferred through air, can have an important and nontrivial impact on the system that might obscure the intrinsic system properties (such as the structure, the degree of order, as well as more subtle details such as the growth kinetics and thermal stability), we provide a detailed description of our sample characterization and preparation procedures.

To minimize these extrinsic factors, the present measurements were performed in a UHV system in which sample cleaning, SAM growth, and structural characterization were all performed in situ without any exposure to the ambient atmosphere. The Au(111) crystal was prepared in an unbaked UHV system with a base pressure of $\sim 10^{-8}$ Torr (the base pressure for this system was $\sim 10^{-10}$ Torr after baking), and was cleaned by successive sputter/anneal cycles using argon ions. This procedure has been found to reliably produce clean and well ordered Au(111) surfaces that have the characteristic $\sqrt{3} \times 23$ surface reconstruction, with surface domain sizes in excess of 2000 Å. In this experiment, the cleanliness was monitored through the S(1s) photoelectron peak. After repeated sputter/anneal cycles, no measurable sulfur signal was observed. In parallel measurements using the same preparation procedure in a separate chamber using, no evidence for contamination could be found with Auger electron spectroscopy.

The monolayer coverage was controlled in-situ through exposure by vapor-phase deposition at room temperature by backfilling the UHV chamber with decanethiol molecules using a previously calibrated leak-valve. In parallel experiments, these growth conditions were determined to lie within the "equilibrium" growth regime, in which the monolayer domain size, $L \geq 2000$ Å, was limited only by the substrate sample quality [55]. During deposition, all filaments in the chamber were turned off, and the ion pump was isolated from the sample chamber. A turbo pump was used to maintain a continuous gas flow during the monolayer growth to prevent any buildup of any contaminants. The exposure was varied over a range of $\sim 10^5$ ($1\ \mathrm{L} = 10^{-6}$ Torr·s) by changing both the exposure time and partial pressure of C10, and all exposures were performed in a pressure range ($P < 5 \times 10^{-5}$ Torr) in which the growth rate has been shown to vary linearly with thiol partial pressure [56]. The absolute exposures were determined after correcting for the ion gauge sensitivity of C10, in which the actual partial pressure was estimated to be approximately one-eighth of the ion gauge reading [56].

Although the XSW measurements were only performed on freshly prepared monolayers, XPS measurements (used to derive the uptake curves)

were performed both on freshly prepared monolayers at a range of converges and on samples perviously analysed with XPS at lower coverages. The high degree of reproducibility implicit in the XPS data with and without a previous X-ray dose provides an independent and sensitive demonstration that the X-ray exposure under our experimental conditions has no significant effect on the monolayer properties.

4. Results

4.1. Evolution of coverage vs. exposure as monitored with XPS

In Fig. 5, we plot the evolution of the S(1s) and Au($3d_{5/2}$) photoelectron intensities for thiol exposures as high as 10_5 L. We have chosen to use a higher photon energy of $E\gamma = 3.136$ eV for the XPS uptake measurements so that the photoelectron yield becomes less sensitive to the molecular orientation and primarily sensitive to the molecular coverage (due to the increased electron mean free path at these energies). As might be expected, the increasing thiol coverage is reflected by both an increase in sulfur signal and a decrease in the Au signal (due to the attenuation of the photoelectrons as they pass through the monolayer). The two-step nature of these date clearly demonstrates that the growth does not proceed by simple Langmuir kinetics, $\Theta(t) = (1 - e^{-t/\tau})$, but instead is well-described by a two-step uptake curve, in which each adsorption step is well approximated by Langmuir kinetics, but with distinct time constants [55] that differ by a factor of ~ 500. It is known that the growth of C10/Au(111) at room temperature involves three phases, and therefore, three time constants might be expected. We use only two time constants here because that is the simplest form compatible with the experimental data. From a least-squares fit of both the S and Au data to the form $A_1[1 - e^{(-t/\tau 1)}] + A_2(1 - e^{(-t/\tau 2)}]$, where t is the exposure in Langmuirs, we find that the two adsorption steps have "time constants" of $\tau_1 = 7.2$ L, and $\tau_2 = 3750$ L.

He diffraction studies first demonstrated that the initial stage of adsorption of thiols on Au(111)

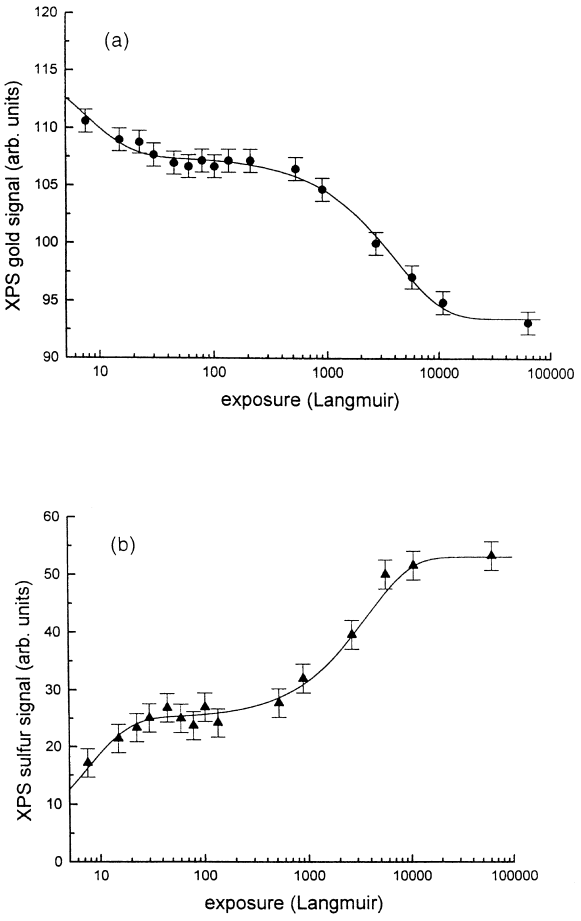

Fig. 5. Evaluation of the photoelectron yields is plotted as a function of thiol exposure for (a) Au-$3d_{5/2}$ and (b) S-1s photoelectron peaks. The solid line is a fit to a two-step adsorption process of the form $A_1[1 - e^{(-t/\tau_1)}] + A_2[1 - e^{(-t/\tau_2)}]$, where t is the exposure in Langmuirs. The decreasing Au signal is due to the attenuation of the photoelectrons due to the adsorption of thiol molecules, and the increasing sulfur signal is due to the increase in thiol coverage.

involves the formation of a "striped phase", in which the molecular axis is parallel to the surface (a "lying down" phase) [57]. Further experiments on the structure of the C10 striped phase by He atom and X-ray diffraction and STM experiments have shown that it forms a $11 \times \sqrt{3}$ unit mesh, having unit cell dimensions of 31.7 Å × 4.997 Å, and containing two molecules per unit mesh [8,55,57–59]. This phase has a nominal coverage of $\Theta = 0.27$ ML ($1\ \text{ML} = 4.62 \times 10^{14}$ molecules

cm^{-2}, which is the density of molecules in the c(4×2) phase). At high coverages, the structure converts to the c(4×2) unit mesh, which is the saturated phase ($\Theta = 1$ ML) with the hydrocarbon axis tilted by $\sim 34^{\circ}$ with respect to the substrate surface normal direction (the "standing-up" phase) [10,37]. A disordered "intermediate phase" also is known to exist for coverages intermediate between the "striped" and c(4×2) phases [55,58]. Consequently, the first adsorption step is associated with the formation of the "lying down" striped phase, followed by a second, slower evolution towards monolayer completion in the "standing up" phase. The evolution of the coverage can therefore be written as

$$\Theta\ (\mathrm{ML}) = 0.27[1 - e^{(-t/7.2)}] + 0.73[1 - e^{(-t/3750)}], \quad (5)$$

which we use to determine the thiol coverage as a function of exposure. Note that the evolution of the photoelectron yield vs. exposure will be similar to that described by Eq. (5), but having coefficients that differ from 0.27 and 0.73 since the photoelectron yield depends upon both the coverage and the attenuation through the monolayer for each phase. This interpretation of the XPS uptake curves is further confirmed by similar measurements using a lower photon energy, $E\gamma = 2630$ eV, in which only the first rapid adsorption step in Eq. (5) is observed in the sulfur photoelectron yield. The lack of second slower adsorption step at this lower energy is due to the increased attenuation within the "standing-up" c(4×2) phase at this lower photon energy, in which the increase in sulfur photoelectron signal as the coverage increases above 0.27 ML is offset by the increased attenuation through the hydrocarbon chains of the c(4×2) phase, resulting in no observable change in the sulfur XPS yield.

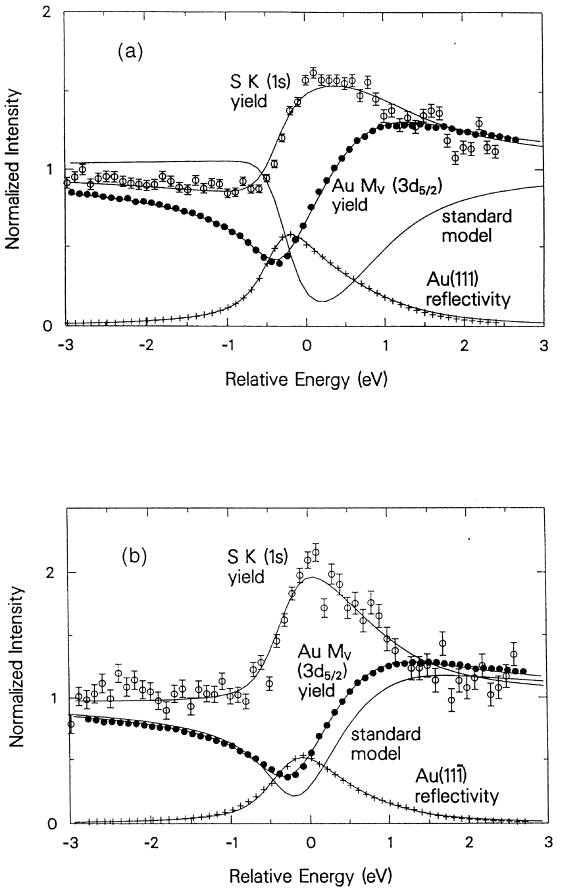

Fig. 6. XSW-induced modulation of the sulfur (open circles) and gold (filled circles) photoelectron yields plotted as a function of photon energy relative to the (111) Bragg condition at $E\gamma = 2632$ eV. The substrate reflectivity is shown as crosses. The data are shown for the (a) (111) and (b) (11-1) Bragg peaks for a saturated monolayer (1.0 ML) in the c(4×2) phase. The solid lines are the best fit to the XSW spectra using the full dynamical theory of X-ray scattering resulting in the XSW parameters summarized in Table 1. Also included in a calculation of the XSW-induced modulation of the sulfur photoelectron yield for the "standard model" based upon the calculation of Sellers et al. [23] in which the sulfur head group bonds in the f.c.c. threefold hollow at a height of 1.905 Å above the Au(111) surface, which should be compared with the open circles.

4.2. XSW results for a complete monolayer ($\Theta = 1$)

We begin the presentation of the XSW measurements by discussing the results for a c(4×2) saturated monolayer formed with an exposure of $\sim 6 \times 10^4$ L at room temperature. In Fig. 6a, we show the S and Au XSW spectra for the C10/Au(111) system measured using the (111) substrate Bragg reflection that is sensitive to the height of the sulfur head group above the Au(111) surface. In each case, the symbols represent the experimental data, and the solid lines are fits to

Table 1
Measured XSW results for the C(4×2) phase at saturation coverage ($\Theta=1$)

	P_{111}	F_{111}	$P_{11\text{-}1}$	$F_{11\text{-}1}$
S(1s)	1.10 ± 0.01	0.41 ± 0.01	0.25 ± 0.01	0.46 ± 0.01
Au($3d_{5/2}$)	-0.1 ± 0.01	0.84 ± 0.01	-0.02 ± 0.01	0.89 ± 0.01

the data using Eq. (1) and the full dynamical theory of X-ray scattering, which directly reveals the coherent position and fraction. For instance, the Au XSW spectrum reveals that the coherent position is $P_{111}(\text{Au})=-0.84\pm0.01$, which reflects the structure of the Au(111) near-surface region (i.e. averaged over the escape length of the photoelectrons) and any imperfections in the substrate lattice. The value of the coherent position suggests that the gold atoms are, on average, located within 1% of the projected bulk lattice sites as would be expected for a bulk-like termination of the Au surface lattice. We have not analyzed these data further due to the complex nature of the substrate lattice relaxations (due to the S–Au interactions) associated with the large c(4×2) unit mesh [9,10].

The fit to the sulfur XSW spectrum reveals a coherent position of $P_{111}=1.10\pm0.01$. If we infer from the Au coherent position that there is little or no vertical relaxation of the Au surface atoms (as is expected for an adsorbate-covered metal surface) [27], the observed coherent position corresponds to an average vertical S–Au spacing of $\langle z\rangle=2.59\pm0.02$ Å. This spacing is significantly larger than the S–Au vertical spacing predicted by quantum chemical calculations, $z=1.9$ Å [23], for a methyl thiolate molecule bound in the f.c.c. threefold hollow site.

We have also obtained similar XSW data for the (11-1) geometry (shown in Fig. 6b), which is accessed by rotating the Au(111) crystal by 70.53° about the [2, −2, 0] crystallographic direction. In the geometry, the XSW spectrum is also sensitive to the lateral sulfur location. From these data, we have determined that the sulfur coherent position is $P_{11\text{-}1}=0.25\pm0.01$, and the coherent fraction is $f_{11\text{-}1}=0.46\pm0.01$. Furthermore, the Au XSW data in the (11-1) geometry reveal a coherent position of $P_{11\text{-}1}(\text{Au})=-0.02\pm0.01$ and a coherent fraction of $f_{11\text{-}1}(\text{Au})=0.89\pm0.01$ that are almost the same values found for the Au XSW results in the (111) geometry. These results are summarized in Table 1.

4.3. Evolution of XSW results vs. coverage

To understand the evolution of the S/Au interface structure through the different coverage-dependent phases (e.g. lying down vs. standing up), we have also used the (111) XSW geometry to probe the sulfur adsorption site at representative thiol coverages. As an example, in Fig. 7, we show the (111) XSW spectra for an exposure of 87 L, which, from Eq. (5), corresponds to a coverage of 0.29 ML. From these data, we have determined that the sulfur coherent position is $P_{111}(0.29\text{ ML})=1.09\pm0.01$, and the coherent fraction is $f_{111}(0.29\text{ ML})=0.41\pm0.01$. Similarly, we have performed experiments at an intermediate thiol exposure of 873 L, corresponding to a coverage of $\Theta=0.42$ ML. Those data (not shown) reveal that the sulfur coherent position is

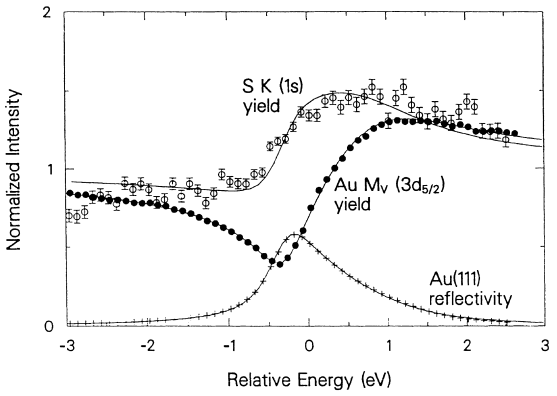

Fig. 7. XSW-induced modulation shown (as in Fig. 6) for the (111) substrate Bragg peak for a coverage of 0.29 ML. The solid lines are the best fit to the XSW spectra. The derived XSW parameters as a function of coverage are summarized in Table 2.

Table 2
Measured XSW results as a function of coverage, Θ

	S(1s)		Au($3_{5/2}$)	
Θ (ML)	P_{111}	F_{111}	P_{111}	F_{111}
0.29	1.09 ± 0.01	0.41 ± 0.01	-0.01 ± 0.01	0.84 ± 0.01
0.42	1.09 ± 0.01	0.60 ± 0.02	-0.03 ± 0.01	0.78 ± 0.01
1.0	1.0 ± 0.01	0.41 ± 0.01	0.01 ± 0.01	0.84 ± 0.01

$P_{111}(0.42\ \text{ML}) = 1.09 \pm 0.01$, and the coherent fraction is $f_{111}(0.42\ \text{ML}) = 0.60 \pm 0.02$. These results are summarized in Table 2.

Independent of the details S/Au interface structure discussed below, these results reveal that the average height (as measured by the coherent position) and the distribution of sulfur positions (as measured by the coherent fraction) is the same at $\Theta = 0.29$ ML and 1.0 ML. Although we have not measured the (11-1) XSW spectra at 0.29 ML, the high precision and sensitivity of the (111) XSW measurement to changes along the surface normal direction (± 0.02 Å) make it extremely unlikely that the S/Au interface structure could have changed (for instance, to a different lateral adsorption site) without any concurrent change in the vertical component interface structure. Since these coverages are very close to the ideal coverages of the "striped" phase (0.27 ML) and the "standing up" c(4 × 2) phase (1.0 ML), we conclude, therefore, that the S/Au interface structures for these two different phases are the same (i.e. within experimental error). Apparently, the differences between the lying-down "striped" phase and the "standing up" c(4 × 2) phase are simply due to the density of absorbed molecules and the orientation of the hydrocarbon axis, and not to changes in the S/Au interface structures.

We note that both the sulfur and gold coherent fractions at $\Theta = 0.42$ ML have changed significantly from those observed at either 0.29 or 1.0 ML, although the coherent positions are unchanged at this coverage. This observation suggests that significant differences exist in the monolayer structure (including the sulfur head group distribution) at that coverage. Although the limited data do not allow us to specify the nature of those changes, we note that diffraction studies have shown that at coverages intermediate between the ideal "striped" phase (0.27 ML) and the c(4 × 2) phase (1.0 ML), a third "intermediate" phase is present that is apparently disordered (i.e. no diffraction peaks are observed with either He atom diffraction or GIXD, and STM also reveals a disordered striped phase) and that has a nominal density of 0.47 ML. This observation suggests that the coherent fraction at 0.42 ML is due primarily to the structure of the intermediate phase that predominates at that coverage, and would suggest, therefore, that the head group structure of the intermediate phase may be different from that of either the striped phase or the c(4 × 2) phase.

5. Derivation of sulphur head group adsorption site(s)

5.1. Models having a unique sulfur site

To interpret the XSW data, we begin by considering the simplest possible model for this system in which all sulfur head groups are located in a single well-defined adsorption site. Within this model, the vertical sulfur position is determined solely by the (111) coherent position and is $z = 2.59 \pm 0.02$ Å. (The XSW result is also consistent with $P_{111} = 0.1$, but this would imply that $z = 0.24 \pm 0.02$ Å which obviously can be ruled out because it leads to a physically impossible Au–S bone lengths of < 1.68 Å.) This vertical S–Au spacing is significantly larger than the value of $z = 1.905$ Å (corresponding to a coherent position of 0.809) predicted theoretically by Sellers et al. [23]. The disagreement can be seen clearly in Fig. 6a in which the XSW induced modulation of the sulfur signal is calculated for the structure predicted by Sellers (standard model). The derived S–Au vertical height of 2.59 Å is also significantly larger than S–metal surface bond lengths [25,27,60,61], which are typically ≤ 2.3 Å.

Having determined the vertical sulfur position through the (111) measurement, the (11-1) coherent position is then determined only by the lateral sulfur binding site (see Fig. 3). Again, we consider first the prediction of the threefold hollow site corresponding to the model of Sellers et al. [23].

In the case of the (111) surface of a face-centered cubic (f.c.c.) crystal, two distinct threefold hollow sites exist, the "h.c.p." and "f.c.c." sites, that are located directly above second- or third-layer Au atoms, respectively. Although these sites are equivalent with respect to the top Au layer, they are distinct with respect to the substrate lattice and are readily distinguished by the XSW technique. Given the measured coherent position of $P_{111}=1.1$, the calculated (11-1) coherent position for an f.c.c. hollow site is $P_{11\text{-}1}=1.03$ (or 0.03), whereas for the h.c.p. site, $P_{11\text{-}1}=0.70$ (or -0.30) as shown in Fig. 3. Both of these values match the measured value of $P_{11\text{-}1}=0.25\pm0.01$ very poorly. The disagreement between this adsorption site and the experimental data can be seen clearly in a calculation of the (11-1) XSW spectra for the model by Sellers et al. [23], in which the sulfur head groups are located in the f.c.c. hollow site having a vertical S–Au spacing of 1.9 Å (standard model in Fig. 6b). The poor level of agreement between these calculated and measured values of the coherent position is a direct and unambiguous demonstration that there is no single sulfur head group located in a threefold hollow site, as is widely asserted in the literature. Other simple binding sites result in a similarly poor agreement with the experimental data. For instance, given that $P_{111}=1.1$, we calculate that a bridge site has coherent position of $P_{11\text{-}1}=-0.13$ (or 0.87), whereas an atop site has $P_{11\text{-}1}=0.36$. Clearly, none of these sites provides an adequate description of the experimental data.

We have also considered the full range of low-symmetry sites by systematically searching for any single site that might be compatible with the experimental data. Although there are low-symmetry sites that reproduce the observed coherent positions ($P_{111}=1.10\pm0.01$ and $P_{11\text{-}1}=0.25\pm0.01$), the predicted coherent fractions for all of these structures can be summarized as: $F_{111}=1$, and $F_{11\text{-}1}<0.35$. Since the product of C and D_H cannot exceed 1.0 (i.e. $CD_H\leq1$), the measured coherent fraction provides a strict lower limit for the geometrical factor a_H. Therefore, we can rule out any single low-symmetry binding site since the measured (11-1) coherent fractions ($f_{11\text{-}1}=0.45\pm0.01$) exceeds the calculated coherent fraction ($f_{11\text{-}1}<0.35$) for all of these low-symmetry structures. Furthermore, inclusion of non-structural contributions to improve the agreement between the calculated and observed values of f_{111} will only increase the disparity between the measured and predicted values of $f_{11\text{-}1}$. Therefore, the XSW results unambiguously rule out any model of this system in which there is only a single sulfur adsorption site.

5.2. Models having two sulfur-binding sites

It is natural to consider the case of two sulfur-binding sites because the symmetry of the X-ray and He atom diffraction patterns and the STM images clearly demonstrates that two distinct molecules exist within the unit mesh (as shown in Fig. 1). The inequivalence of these two molecules and the strictly equal number of each of the two molecules within the unit mesh are therefore both defining characteristics of the $c(4\times2)$ unit mesh symmetry. Consequently, we use this information as an externally imposed constraint in the XSW analysis to determine, first of all, whether the inequivalence of the sulfur head groups of these two molecules should be described as a perturbation about a single well-defined site or as two distinct binding sites and, secondly, to determine the precise sulfur adsorption sites.

Within the context of a two-binding-site model, the measured coherent positions provide a direct measure of the average position of the two sulfur head groups projected along the respective crystallographic directions. We begin by discussing the height of the two sulfur atoms, since P_{111} is sensitive to the average vertical height of the sulfur head groups. As discussed in Section 2, as the width of the sulfur height distribution increases, the coherent fraction will decrease. Consequently, the low observed value of $f_{111}=0.41\pm0.01$ may be due to different heights of the two sulfur head groups. In the case of two sulfur atoms, the geometrical factor decreases as a function of the displacement, Δ, of each sulfur head group about their mean position, as $a_H=\cos(2\pi\Delta/d_H)$. If we assume that $f_{111}=a_{111}$ (i.e. $CD_{111}\sim1$), then the observed coherent fraction $f_{111}=0.41$ corresponds to a displacement of $\Delta=0.43$ Å. This implies that

two very different vertical S–Au spacings exist: $z = 2.59 \pm \Delta = 2.16$ Å and 3.02 Å. [Again, the XSW results are degenerate to within the period of XSW field so that both of these heights can be modified by the period of the standing wave (± 2.355 Å), although this modification results in physically unrealistic S–Au vertical distances]. Before we can conclude that the derived value of Δ is representative of the sulfur head group structure, we must also consider values of $CD_{111} < 1$. As the product CD_{111} is reduced below 1.0, the derived value of Δ will decrease. Consequently, at this point in the analysis, we can only place an upper limit on the magnitude of Δ (i.e. $\Delta \geq 0.43$ Å).

A large difference in heights, as suggested above, would already imply that the two sulfur head groups are likely to be found in different lateral adsorption sites. We will now quantitatively address the question of which lateral adsorption sites are consistent with the XSW data. To explore the full range of sulfur head group locations systematically, we follow a similar analysis method to that used previously by Berman et al. [62] to determine the location of a single low-symmetry adsorption site using XSW. To do this, we fix the vertical height of each of the two sulfur head groups as determined above using the measured (111) coherent fraction, so that the only adjustable parameters are the lateral positions of the two sulfur head groups and the product of CD_H. For simplicity, we begin by assuming that $C = D_H = 1$ (i.e. $a_{111} = f_{111}$), and perform a grid search over the full range of lateral sulfur positions for which the coherent fractions and positions are consistent with the experimental data (we discuss the possibility in which non-structural contributions are significant in detail below). For the coherent positions, we search for structures that reproduce the observed values to within one standard deviation, σ, of the derived value, i.e. a calculated coherent position is considered acceptable if $P - 0.01 \leq P_{\text{calc}} \leq P + 0.01$. Since non-structural contributions to the coherent fraction may be present and will have the effect of increasing the value of a_H beyond the statistical uncertainty of that parameter, we have increased the upper range of acceptable coherent fractions to be: $f_{11\text{-}1} - 0.01 \leq a_H \leq f_{11\text{-}1} + 0.09$. This range takes into account the possibility of systematic error in the analysis caused by the presence of non-specifically bound sulfur (because for a given measured $f_H = CD_H a_H$, $a_H \leq f_H$ for $CD_H \leq 1$).

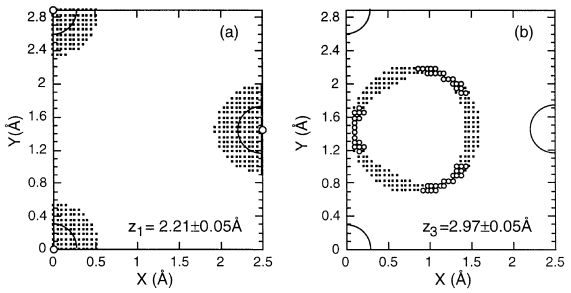

Fig. 8. Detailed map of the positions of each of the two sulfur head groups at heights of (a) $z_1 = 2.21 \pm 0.05$ Å and (b) $z_3 = 2.97 \pm 0.05$ Å with respect to the underlying substrate lattice that are consistent with the XSW data for $\Theta = 1.0$ ML. The small dots represent the range of allowed sites of each sulfur head group for any position of the other sulfur head group, and the large circles denote the Au substrate lattice sites. To demonstrate the correlations present in these date explicitly, we also show as open circles the allowed sulfur head group locations (at $z_3 = 3.02$ Å) when the other sulfur head group (at $z_1 = 2.16$ Å) is restricted to the atop site ($x = 0$, $y = 0$).

The result of this search is summarized in Fig. 8. The plotted points are head group positions that are compatible with the experimental data, and the large circles are the substrate Au atom locations. Due to the different heights of the two sulfur head groups, the XSW results are sensitive to the lateral position of each of the individual sulfur head groups. Consistent with our discussion above concerning models containing only a single sulfur head group, no structures are compatible with either of the two sulfur head groups located in the threefold hollow site (either f.c.c. or h.c.p.). Instead, the first sulfur head group is found at a vertical height of $z_1 = 2.16$ Å, and is determined to have a lateral location, R_{xy}, within 0.5 Å of an atop site (Fig. 8a). The second sulfur head group (molecule 3, as shown in Fig. 1) is found at a vertical height of $z_3 = 3.02$ Å and is located within an annulus surrounding the f.c.c. threefold hollow site ($R_{xy} = R_{\text{f.c.c.}} + \delta_3$, 0.6 Å $\leq \delta_3 \leq$ 0.8 Å) as shown in Fig. 8b. Because correlations between the two head group positions are implicit in these data, we emphasize that the allowed position of each sulfur head groups is only valid for a subset of the other

head groups positions. This is shown explicitly for the exemplary case in which the sulfur head group (at $z_1 = 2.16$ Å) is restricted to an atop site (small open circle, Fig. 8a), and the acceptable lateral locations of the other sulfur head group (at $z_3 = 3.02$ Å) are plotted (open circles, Fig. 8b).

We have yet to explore structures in which $CD_H < 1$ in deriving Fig. 8. It is necessary, therefore, to perform similar searches for particular values of the product CD_H over the full allowable range, $0.46 \leq CD_H \leq 1.0$ because the value of CD_H will impact on the derived value of Δ (i.e. the vertical heights of the two sulfur head groups), that will then impact on the derived (11-1) coherent position. Upon doing this, we note that this simply has the effect of reducing the range of allowable sulfur head group sites shown in Fig. 8, without the introduction of any new sites. Furthermore, we find that no structures are compatible with the XSW results for $CD_H < 0.65$. Therefore, values of $CD_H < 1.0$ only reduce the range of allowable structures but do not in any way change the conclusions. Consequently, the results in Fig. 8 unambiguously reflect the full range of possible lateral sites for each of the two distinct sulfur head groups, so that all other head group sites are incompatible with the XSW data. If we take into account the full range of structures that are compatible with the XSW data, we find that:

$z_1 = 2.21 \pm 0.05$ Å, $R1_{xy} = R_{\text{atop}} + \delta_1$

with $|\delta_1| \leq 0.5$ Å, and

$z_3 = 2.97 \pm 0.05$ Å, $R3_{xy} = R_{\text{f.c.c.}} + \delta_3$

with 0.6 Å $\leq |\delta_3| \leq 0.8$ Å, where δ_i reflects the lateral displacement of each head group from a high-symmetry site.

Although the results in Fig. 8 represent the position of each sulfur head group with respect to the Au substrate lattice, we can also determine which spacings between the two sulfur head groups are compatible with the XSW data through the correlations in the two sulfur head group positions implicit in Fig. 8. The full range of allowed S–S spacings [as a function of $(x_3 - x_1)$ and $(y_3 - y_1)$] compatible with the XSW data is shown in Fig. 9. In this plot, all information concerning the lateral relationship between the sulfur head groups and the Au substrate lattice is lost, and the shaded regions are ones in which the magnitude and orientation of the vector separating the two sulfur head groups are compatible with the XSW data. As might be expected, because of the indirect sensitivity of XSW to the S–S spacing, the range of S–S spacings and orientations is rather broad. In spite of this, the data clearly demonstrate that the XSW data are inconsistent with an S–S spacing that is 5 Å along next-nearest-neighbour direction of the Au substrate (open circle, Fig. 9), as is widely assumed in the literature, and as directed by $\sqrt{3} \times \sqrt{3}$R30° overlayer symmetry (independent of the actual sulfur binding site).

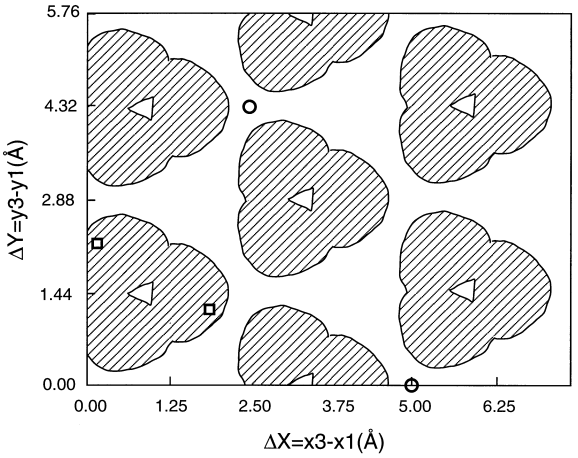

Fig. 9. Range of relative lateral S–S spacings (of molecule 3 with respect to molecule 1) that are consistent with the XSW data, plotted as shaded regions as a function of the $\Delta X = x_3 - x_1$ and $\Delta Y = y_3 - y_1$, and derived on the basis of the correlations of the sulfur head group positions implicit in Fig. 8. These data are consistent with the S–S spacing derived on the basis of the GIXD results (open squares) but are inconsistent with a 5 Å S–S spacing as dictated by a $\sqrt{3} \times \sqrt{3}$R30° symmetry (open circles).

6. Interpretation of results

6.1. Comparison to related sulfur-containing systems

Because the XSW data clearly contradict the most fundamental tenet of the "standard" model

(i.e. a single sulfur head group location), because no independent experimental evidence exists to support the notion of bonding in the threefold hollow site, and because the XSW data are inconsistent with an S–S spacing of 5 Å in the orientation dictated by a $\sqrt{3}\times\sqrt{3}R30^\circ$ structure, we conclude that the "standard" model is inappropriate for the Cn/Au(111) system. To achieve a coherent picture of this system, we must now develop a model in which the two sulfur head groups are located in different lateral and vertical locations.

To gain insight into the nature of the bonding between the sulfur head group and the Au substrate, we first compare our results to the chemisorption of thiols and atomic sulfur on other metal surfaces. For example, methanethiol (C1) on Ni(111) has a S–Ni bond length of 2.24 Å [61], whereas for sulfur on Ni(111), the S–Ni bond length is 2.13 Å [25]. In the case of C1/Cu(111), the S–Cu bond length is found to be 2.38 Å [60]. Even for the case of sulfur adsorption on the open face of Cu(001), the S–Cu bond length is found to be 2.25 Å [27]. Although the sulfur atom was located in a hollow site in all of these cases (and therefore may not be directly comparable with the present results), they all have bond lengths that are very similar to that derived for the sulfur head group in the atop site (molecule 1), which has an S–Au distance of 2.16 Å, but are all much smaller than the minimum S–Au separation for the other head group (molecule 3), which is 3.1. Å [i.e. $(2.97^2+0.9^2)^{1/2}$].

Further insight may be found by comparing the XSW results to bond lengths found in bulk organometallic compounds. Here, we find that the derived S–Au distance in the atop site (2.16 Å) is somewhat smaller than bulk S–Au "bonding" distances that are observed in the range of 2.28–2.35 Å [63–65] and as high as 2.5 Å [66]. Differences at this level are not surprising given the difference of bonding sulfur to metal atom vs. bonding to a metal surface. In contrast, the smallest S–Au distance of the second sulfur head group (3.1 Å) is clearly outside the range of observed bonding distances, but instead is very similar both to the observed "non-bonding" distances (3.1 Å), and to the sum of the van der Waals radii of sulfur and Au atoms (3.5 Å) [66]. Taken together, these results suggest two important observations: (1) the derived sulfur locations results in S–Au distances that are both physically and chemically reasonable in comparison to other related S–metal systems, and (2) the derived S–Au distances suggest that a chemical bond exists between the sulfur head group located in the atop site (molecule 1) and the Au substrate atom directly below it, and there is apparently no direct chemical interaction between the second sulfur head group (molecule 3) and the Au substrate.

6.2. Comparison to "sulfur pairing" models

While some residual ambiguity of the XSW results clearly remains concerning the exact S/Au interface structure, the XSW results can be used to quantitatively test the validity of any other proposed structures. We therefore discuss the XSW results in the context of a "sulfur pairing" model, which is the only other structure that has been proposed for the Cn/Au(111) system. In this model, the S–S spacing was determined to be 2.2 Å, with the S–S "bond direction" having an angle of 3° with respect to the Au nearest-neighbour direction. In Fig. 9, this S–S spacing is superimposed on those that were found to be compatible with the XSW results, and is clearly consistent with the range of S–S spacings derived from the XSW data.

The only apparent contradiction between the GIXD and XSW results is found in the adsorption site of the molecules with respect to the Au substrate lattice. The GIXD results reported [9] a best fit when the two sulfur head groups were located near the threefold hollow and bridge sites, which are inconsistent with the XSW data (as shown in Fig. 8). However, it must be noted that these techniques probe the S/Au interface in very different ways. The XSW technique is directly sensitive to the S adsorption site with respect to the substrate lattice and is relatively insensitive to the actual S–S spacing (see Figs. 8 and 9), and the GIXD results are primarily sensitive to the S–S spacing, with substantially less sensitivity to the lateral adsorption site. To demonstrate this latter

point explicitly, we have performed structure factor calculations of different structural models that we compare with the GIXD data [9,31]. For instance, a comparison of the GIXD data with calculations for the best-fig (''sulfur-pairing'') structure reveals a quality of fit of

$$S\chi^2 = (1/n)\sum[(I_{\text{exp}} - S^* I_{\text{calc}})/\sigma_{\text{exp}}]^2 = 1.9$$

where I is the X-ray scattering intensities (experimental and calculated), σ is the statistical uncertainty in the measured intensity, and S is a scale factor), whereas the best-fit for a fully optimized ''standard'' model has $S\chi^2 = 16$. In comparison, by modifying the best fit ''sulfur pairing'' model by rigidly translating the sulfur ''dimer'' (i.e. without any change in the S–S spacing), we can create a model that is fully consistent with the XSW data. After allowing optimization of the other aspects of the structure, we find a quality of fit of $S\chi^2 \leq 2.5$. Although an exhaustive simultaneous optimization of both the XSW and GIXD data has yet to be performed, these numbers clearly demonstrate the primary sensitivity of GIXD to the S–S distance and orientation, and its secondary sensitivity to the lateral site. In the present context, it is sufficient to note that the above calculations prove that no inherent contradiction exists between the sulfur-pairing model as derived by GIXD and the XSW results.

6.3. Discussion of XSW results and synthesis of a structural model

We can now try to synthesize a model. Since the XSW results clearly imply that although one sulfur head group (at $z_1 = 2.2 \pm 0.05$ Å) is directly bound to the Au surface, the other (at $z_3 = 2.97 \pm 0.05$ Å) is not. It is natural, therefore, to discuss these results in the context of a ''sulfur-pairing'' model in which the head group structure is in the form of a sulfur dimer moiety that is bound to the surface through only one of the two sulfur head groups (that located in the atop site). A schematic of this structure is shown in Fig. 10. Using a lateral distance between the two head groups consistent with both the XSW data and the GIXD data (2.2 Å), and using the difference

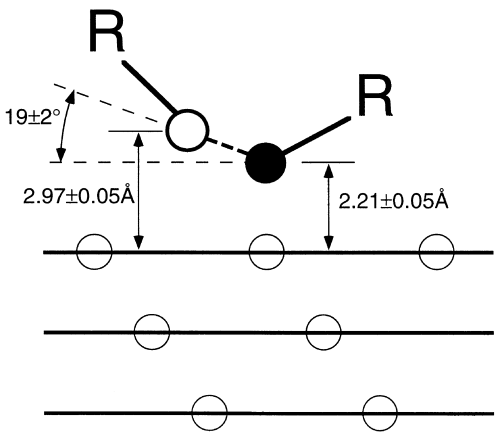

Fig. 10. Schematic of the derived ''sulfur-dimer'' structure, revealing that although one of the two head groups interacts directly with the substrate (filled circle), the other head group does not (open circle). The hydrocarbon chains are schematically shown as ''R''. From the lateral S–S spacing consistent with both the GIXD and XSW date (2.2 Å) and their heights as derived by XSW, we derive a tilt of the S–S ''bond'' (shown as a dashed bold line) of $19 \pm 2^\circ$ away from the Au surface plane.

in vertical heights as derived by XSW ($\Delta z = 0.76 \pm 0.1$ Å, as discussed in Section 5.2), we therefore derive the angle of tilt of the S–S ''bond'' to be $19 \pm 2^\circ$ above the Au surface plane. This corresponds to an angle of $109 \pm 2^\circ$ with respect to the Au–S bond (assuming that the sulfur head group is located exactly in the atop site) that is consistent with the tetrahedral bond angle (109.4°), and suggests a lone-pair interaction between the two sulfur head groups as a possible explanation for the sulfur dimer structure.

The sulfur dimer model is appealing because it provides a simple explanation for a number of diverse experimental facts known about this system. First of all, because the model suggests that the molecules are bound to the Au surface as a dimer, there would be no reason to expect two distinct desorption temperatures (in contrast to any models that might explain the XSW results in the context of two distinct uni-molecular adsorption sites). Furthermore, it is known from temperature-programmed desorption (TPD) experiments that the desorption product is a disulfide for chain lengths ranging as low as C1 [67] to at least as high as C18 [68]. Although this has been interpre-

ted in the context of second order desorption of thiolates, it might also be reasonable to associate the desorption product (in the context of the XSW results) with the first-order desorption of adsorbed dimers. Furthermore, recent studies have shown that a bimolecular adsorption mechanism exists in the growth of C10/Au(111) by vapor deposition [56]. The dimer structure also provides a very simple and elegant explanation for the presence of the unit cell doubling present in both the $c(4\times2)$ and striped phases [8,9,32,57–59] (see Section 6.4 for more detail).

It has also been found that SAMs formed from either thiols or disulfides result in indistinguishable monolayers [69]. This observation had been interpreted in the context of the "standard model" as a result of the dissociative adsorption of the disulfide molecule, although such an observation is also consistent with a "dimer" adsorption structure. Perhaps the only experimental evident that might be interpreted as being contrary to a sulfur dimer head group structure is that concerning mixed monolayers, in which exchange has been observed between adsorbed asymmetric disulfides [70]. Although those studies were performed on evaporated Au films [and therefore may not be directly comparable to our studies on Au(111) single crystalline surfaces], those results are not inconsistent with a dimer adsorption structure as long as the barrier for S–S bond cleavage on the surface is not too high. In this context, given the XSW result that the S/Au interface structure is different in the "intermediate phase" than in either the $c(4\times2)$ or striped phase, and given the presence of a melted phase over a broad range of the (Θ, T) phase diagram in this system (include room temperature at submonolayer coverages) [55], there is no reason to assume a priori that sulfur dimers necessarily exist as stable units in either or both of these phases.

We can also discuss these results in the context of the XPS binding energies for this system. From the observed decrease in the S(2p) XPS binding energy of the final chemisorbed species ($E_b = 162.7$ eV) with respect to the physisorbed disulfide ($E_b = 164.8$ eV) [67], it can be inferred that if the adsorption is in the form of a disulfide, then the S–S bond should be reduced, and consequently the S–S bond length would be expected to be longer (J. Schwartz, pers. commun.; [71]) than that found in an isolated disulfide compound (2.0 Å) [33]. Given the lateral S–S spacing measured by GIXD (2.2 Å) and the measured difference in height of the two sulfur head groups (0.76 Å), this results in an S–S "bondlength" of 2.33 Å, which is consistent with the notion of a reduced S–S bond. In terms of the sensitivity of XPS to the sulfur adsorption site, note also that in a closely related system [perfluorinated thiols adsorbed on Au(111)], it was found that the monolayer structure was incommensurate with the substrate lattice, which immediately implies the existence of multiple binding sites [72]. However, a recent XPS study of that system finds no evidence for any splitting or broadening of the S(2p) photoelectron peak for the perfluorinated thiol monolayer [73], which suggests that the sulfur XPS binding energy may be insensitive to the actual binding site in the S/Au(111) system.

In comparing our results with other closely related surface adsorption systems, we note that sulfur has been previously observed to form S_8 rings on Au(111) surfaces under electrochemical conditions [74] with an internal S–S spacing of 2.5 Å. This observation clearly demonstrates the ability of sulfur to form similar structures on Au(111) surfaces. Furthermore, the isoelectronic Te/Au(111) and Au(001) systems are known to exhibit a number of complex structures, which have been interpreted in the context of unit meshes that contain multiple Te dimers [75,76], and which are strikingly similar to the $c(4\times2)$ unit mesh, as shown in Fig. 1. Clearly, the sulfur dimerization that we propose for the C10/Au(111) system is not unprecedented. It is also interesting to note that although no direct experimental evidence has been reported to support independently the notion of an S–S "bond" in the C10/Au(111) system, recent Raman spectroscopy studies have shown the existence of an unexpected and possibly novel resonant Raman process. This process has been determined to be due to an electronic interaction at the S/Au interface and might therefore be associated with the presence of a sulfur dimer species (B. Gregory, pers. commun.).

6.4. Discussion of the coverage dependence

In light of our observation that the local S/Au interface structure of the low-coverage "striped" phase ($\Theta = 0.27$ ML) and the c(4 × 2) phase ($\Theta =$ 1 ML) are indistinguishable as measured by XSW, we now compare their two-dimensional structures. A schematic of these two structures if found in Fig. 11a and b, in which the unit cell size and symmetry are determined solely from the diffraction pattern symmetry of each phase. In both phases, the hydrocarbon chains are shown as shaded regions [which, in the "standing up" c(4 × 2) phase, are schematically shown as shaded circles] and the head group positions (small filled circles) are shown consistent with the combined XSW and GIXD results incorporating an S–S spacing of ~2.2 Å. Note that He diffraction measurements of the striped phase unit mesh as a function of chain length have previously determined that the length of the unit mesh is quantitatively consistent with the length of the C10 molecules, its van der Waals radii, and the S–S spacings derived from the GIXD data [59].

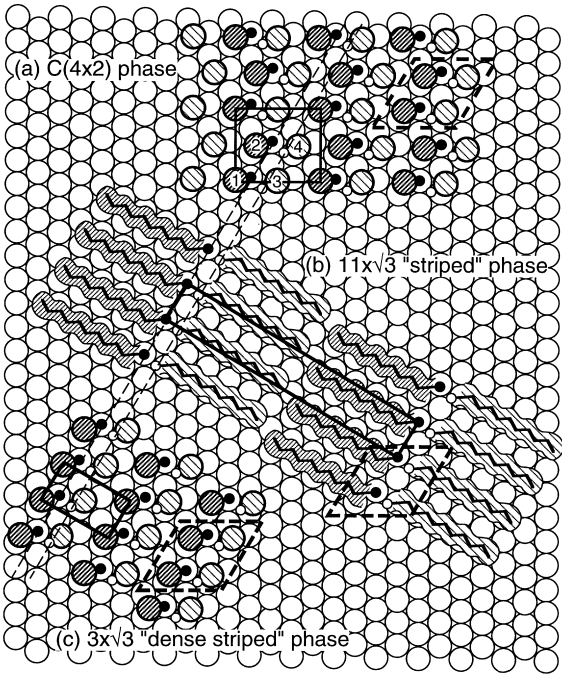

Fig. 11. Schematic of the relationship between (a) c(4 × 2) phase at 1.0 ML, (b) striped phase at 0.27 ML, and (c) fictitious "dense striped" phase that has the same density and local head group structure as the c(4 × 2) phase. The dashed line is a guide to the eye to accentuate the similarities and differences between those structures, and the hydrocarbon chains are denoted by the shaded regions for both the "striped" phase, and the c(4 × 2) phase (where the chains are schematically shown as filled circles). Note that the c(4 × 2) phase and the fictitious "dense striped" phases differ only in the packing of the "supramolecular aggreates" shown schematically as dashed parallelograms.

From this schematic, the similarities of the two phases are readily apparent. Even without the XSW results, the presence of "pairing" of adjacent molecules is apparent for both the c(4 × 2) and the striped phases solely on the basis of the unit cell symmetry and size, and this similarity would immediately suggest a fundamental connection between the head group structure of the two phases. Furthermore, the spacing of the sulfur head groups along the short axis of the striped phase (5.0 Å, along the dashed line in Fig. 11) is identical to the relationship between molecules 1 and 2 in the c(4 × 2) phase as shown in Fig. 1 (the latter being dictated by the absence of certain diffraction peaks in the c(4 × 2) phase). Finally, our determination that the head group structures of the striped and c(4 × 2) phases are equivalent as measured by XSW suggests that molecules 1 and 3 have the same spatial relationship in these two very different phases.

There are also interesting differences between the two phases. Given that the head group structures for the striped and c(4 × 2) phases are indistinguishable with XSW, one might expect initially that the c(4 × 2) phase could be created by simply the "standing up" of the hydrocarbon chains and reducing the long axis of the striped phase unit mesh to maximize the coverage. To show clearly that this is not how the c(4 × 2) phase is obtained, we show a schematic of such a fictitious "dense striped" phase (Fig. 11c), which has the same molecular density as the c(4 × 2) phase, but whose symmetry instead resembles the orthorhombic packing found in odd-chain-length alkane crystals. Although the 5.0 Å spacing of these striped phases continues indefinitely along the dashed lines in Figs. 11b and c, this relationship within the c(4 × 2) phase (Fig. 11a) instead is modulated

about the vertical axis, resulting in the zigzag pattern of light and dark molecules.

We note that all three structures shown in Fig. 11 can be constructed from the same four-molecule "supramolecular aggregate" (corresponding to molecules 1–4 in Fig. 11a, and shown schematically by the dashed parallelograms in Fig. 11a–c). Because the c(4×2) phase and the dense striped phase are both constructed from the same S/Au interface structure, these structures differ only in the relative packing of the supramolecular aggregates. This clearly implies that the hydrocarbon chain packing between neighbouring supramolecular aggregates is the driving force behind the modulation that results in the c(4×2) unit mesh. In other words, the essential element that is necessary to explain the stability of the c(4×2) phase with the respect to other structures (such as the dense striped phase) appears to be the steric packing constraints of the hydrocarbon chains when constrained by the presence of a dimerization of the sulfur head groups. In this respect, it is not surprising that Goddard et al. [39] were able to reproduce the observed c(4×2) structure by assuming the existence of an S–S "bond".

7. Conclusions

Using the technique of XSW, we have determined that the sulfur head group structure of C10/Au(111) is not described by a unique sulfur bond in the threefold hollow site of the gold surface, but instead have revealed that two distinct sulfur head group sites exist. Whereas one sulfur head group is laterally located with 0.5 Å of an atop site with a vertical height above the Au(111) lattice plane of 2.21 ± 0.05 Å, the other is found in an annulus surrounding the f.c.c. hollow site with a vertical height of 2.97 ± 0.05 Å. These S–Au distances immediately suggest that although the first sulfur head group is directly bound to the Au(111) surface, no S–Au bond exists for the other sulfur head group. The results have been interpreted in the context of the "sulfur-pairing model" previously derived on the basis of the GIXD data, and suggest that the thiol molecules are bound to the surface in the form of an asymmetrical dimer that is bound primarily through only one of the two sulfur head groups in the dimer and is tilted with respect to the surface plane by $19 \pm 2°$.

By performing XSW measurement as a function of the thiol coverage, we have also determined that the sulfur head group structure for the lying-down striped phase (at $\Theta = 0.27$ ML) is indistinguishable from that of the saturated c(4×2) structure found (at $\Theta = 1.0$ ML). This observation suggests that the primary difference between these two phases is in the orientation of the hydrocarbon axis (and the related molecular coverage) and is not due to changes in the S/Au interface structure. From this, we suggest that the known symmetry of the c(4×2) phase is stabilized by the packing of a neighbouring four-molecule supramolecular aggregate that is common to these two structures.

Although a large gulf remains between our experimental results and recent results using theory and MD simulation, we hope that the present work will stimulate new theoretical attention aimed not only at resolving the complexities of the structure of this model system, but also at the more pressing issue of developing a more fundamental understanding of self-assembly processes in general.

Acknowledgements

We would like to acknowledge Barry Karlin for experimental assistance at the X24A beamline at the NSLS. One of us (P.F.) would like to acknowledge useful and insightful conversations with Ariane Eberhardt, Jeffrey Schwartz, Brian Gregory and Robert Whetten, and we would like to thank Brian Gregory for sharing his unpublished data. This work was supported by DOE grant DE-FG02-93ER45503, DOE contract W31-109-ENG-38 at Argonne National Laboratory, and F.S. acknowledges the support of the DFG (SCHR 537/2-1). Some work was performed at the NSLS, which is supported by DOE Contract DE-AC0276CH-00016.

References

[1] L.H. Dubois, R.G. Nuzzo, Annu. Rev. Phys. Chem. 43 (1992) 437.
[2] A. Ulman, An Introduction to Organic Films, Academic Press, San Diego, CA, 1991.
[3] J.D. Swalen, D.L. Allara, J.D. Andrade et al., Langmuir 3 (1987) 932.
[4] G.M. Whitesides, P.E. Laibinis, Langmuir 6 (1990) 87.
[5] C.A. Alves, E.L. Smith, M.D. Porter, J. Am. Chem. Soc. 114 (1992) 1222.
[6] E. Delmarche, B. Michel, H.A. Biebuyck et al., Adv. Mater. 8 (1996) 719.
[7] G.E. Poirier, M.J. Tarlov, Langmuir 10 (1994) 2853.
[8] G.E. Poirier, M.J. Tarlov, H.E. Rushmeier, Langmuir 10 (1994) 3383.
[9] P. Fenter, A. Eberhardt, P. Eisenberger, Science 266 (1994) 1216.
[10] P. Fenter, P. Eisenberger, K.S. Liang, Phys. Rev. Lett 70 (1993) 2447.
[11] N.C. Camillone III, C.E.D. Chidsey, G.-Y. Liu et al., J. Chem. Phys. 98 (1993) 3503.
[12] N.C. Camillone III, C.E.D. Chidsey, G.-Y. Liu et al., J. Chem. Phys. 94 (1991) 8493.
[13] G. Hahner, M. Kinzler, C. Thummler et al., J. Vac. Sci. Technol. A 10 (1992) 2758.
[14] M.S. Yeganeh, S.M. Dougal, R.S. Polizzotti et al., Phys. Rev. Lett. 74 (1995) 1811.
[15] L.H. Dubois, B.R. Zegarski, R.G. Nuzzo, J. Chem. Phys. 98 (1993) 678.
[16] C.D. Bain, E.B. Troughton, Y.-T. Tao et al., J. Am. Chem Soc. 111 (1989) 321.
[17] R.G. Nuzzo, L.H. Dubois, D.L. Allara et al., J. Am. Chem. Soc. 112 (1990) 558.
[18] P.E. Laibinis, G.M. Whitesides, D.L. Allara et al., J. Am. Chem. Soc. 113 (1991) 7152.
[19] A. Ulman, Chem. Rev. 96 (1996) 1533.
[20] F. Balzer, R. Gerlach, G. Polanski et al., Chem. Phys. Lett. 274 (1997) 145.
[21] C. Shonenberger, J. Jorritsma, J.A.M. Sondag-Huethorst et al., J. Phys. Chem. 99 (1995) 3259.
[22] W.B. Caldwell, D.J. Campbell, K. Chen et al., J. Am. Chem. Soc. 117 (1995) 6071.
[23] H. Sellers, A. Ulman, Y. Shnidman et al., in: P.S. Bagus, F. Parmigiani, G. Pacchioni (Eds.), Cluster Models for Surface and Bulk Phenomena, Plenum, New York, 1992.
[24] M.A. Van Hove, G.A. Somorjai, Surf. Sci. 299–300 (1994) 487.
[25] Y. Kitajima, S. Yagi, T. Yokoyama et al., Surf. Sci. 320 (1994) L89.
[26] D.F. Ogletree, R.Q. Hwang, D.M. Zeglinski et al., J. Vac. Sci. Technol. B 9 (1991) 886.
[27] Q.T. Jiang, P. Fenter, T. Gustafsson, Phys. Rev. B 42 (1990) 9291.
[28] C. Zeng, R.A. McFarlane, K.A.R. Mitchell, Surf. Sci. 177 (1986) 329.
[29] L. Strong, G.M. Whitesides, Langmuir 4 (1988) 546.
[30] G.-Y. Liu, M.B. Salmeron, Langmuir 10 (1994) 367.
[31] P. Fenter, in: A. Ulman (Ed.), Thin Films: Self-Assembled Monolayers of Thiols, Academic Press, San Diego, CA, 1998.
[32] B. Beagley, K.T. McAloon, Trans. Faraday Soc. 67 (1971) 3216.
[33] K.M. Beardmore, J.D. Kress, A.R. Bishop et al., Synthet. Metals 84 (1997) 317.
[34] A.J. Perstin, M. Grunze, Langmuir 10 (1994) 3668.
[35] R. Bhatia, B.J. Garrison, Langmuir 13 (1997) 4038.
[36] P. Fenter, A. Eberhardt, K.S. Liang et al., J. Chem. Phys. 106 (1997) 1600.
[37] R. Bhatia, B.J. Garrison, Langmuir 13 (1997) 765.
[38] N.C. Camillone III, C.E.D. Chidsey, P. Eisenberger et al., J. Chem. Phys. 99 (1993) 744.
[39] J.J. Gerdy, W.A. Goddard III, J. Am. Chem. Soc. 118 (1996) 3233.
[40] A. Nilsson, M. Wienelt, T. Wiell et al., Phys. Rev. Lett. 78 (1997) 2847.
[41] C.B. Duke, Surf. Sci. 299–300 (1994) 24.
[42] J. Zegenhagen, Surf. Sci. Rep. 18 (1993) 199.
[43] D.P. Woodruff, D.L. Seymour, C.F. McConville et al., Phys. Rev. Lett. 58 (1987) 1460.
[44] T.-L. Lee, Y. Qian, M.J. Bedzyk, Physica B 221 (1996) 437.
[45] M.J. Bedzyk, G.M. Bommarito, J.S. Schildkraut, Phys. Rev. Lett. 62 (1989) 1376.
[46] M.J. Bedzyk, D.H. Bilderback, G.M. Bommarito et al., Science 241 (1988) 1788.
[47] B.W. Batterman, Phys. Rev. Lett. 22 (1969) 703.
[48] H. Rieley, G.K. Kendall, A. Chan et al., Surf. Sci. 392 (1997) 143.
[49] B.W. Batterman, H. Cole, Rev. Mod. Phys. 36 (1964) 681.
[50] P.L. Cowan, S. Brennan, R.D. Deslattes et al., Nucl. Instrum. Meth. A 246 (1986) 154.
[51] I.M. Tidswell, T.A. Rabedeau, P.S. Pershan et al., J. Chem. Phys. 95 (1991) 2854.
[52] J. Li, K.S. Liang, G. Scoles et al., Langmuir 11 (1995) 4418.
[53] P.E. Laibinis, R.L. Graham, H.A. Biebuyck et al., Science 254 (1991) 981.
[54] M. Wirde, U. Gelius, T. Dunbar et al., Nucl. Instrum. Meth. Phys. Res. B 131 (1997) 245.
[55] F. Schreiber, A. Eberhardt, S. Wetterer et al., Phys Rev. B 57 (1998) 12476.
[56] A. Eberhardt, P. Fenter, P. Eisenberger, Surf. Sci. 397 (1998) L285.
[57] N.C. Camillone III, P. Eisenberger, T.Y.B. Leung et al., J. Chem. Phys. 101 (1994) 11031.
[58] G.E. Poirier, E.D. Pylant, Science 272 (1996) 1145.
[59] N.C. Camillone III, T.Y.B. Leung, P. Schwartz, Langmuir 12 (1996) 2737.
[60] N.P. Prince, D.L. Seymour, D.P. Woodruff et al., Surf. Sci. 215 (1989) 566.
[61] A. Fernandez, J.P. Espinos, A.R. Gonzalez-Elipe et al., J. Phys. Cond. Matt. 7 (1995) 7781.
[62] L.E. Berman, B.W. Batterman, J.M. Blakely, Phys. Rev. B 38 (1988) 5397.

[63] W. Wojnowski, B. Becker, J. Sassmannshausen et al., Z. Anorg. Allg. Chem. 620 (1994) 1417.
[64] P.J. Bonasia, D.E. Gindelberger, J. Arnold, Inorg. Chem 32 (1993) 5126.
[65] G. Marbach, J. Straehle, Angew. Chem. 23 (1984) 715.
[66] P. Pyykko, Chem. Rev. 97 (1997) 597.
[67] R.G. Nuzzo, B.R. Zegarski, L.H. Dubois, J. Am. Chem. Soc. 109 (1987) 733.
[68] N. Nishida, M. Hara, H. Sasabe et al., Jpn. J. Appl. Phys. 35 (1996) L799.
[69] H.A. Biebuyck, C.D. Bain, G.M. Whitesides, Langmuir 10 (1994) 1825.
[70] H.A. Biebuyk, G.M. Whitesides, Langmuir 9 (1993) 1766.
[71] L.C. Pauling, The Nature of the Chemical Bond and the Structure of Molecules and Crystals: An Introduction to Modern Structural Chemistry, Cornell University Press, Ithaca, NY, 1940.
[72] G.-Y. Liu, P. Fenter, C.E.D. Chidsey et al., J. Chem. Phys. 101 (1994) 4301.
[73] D.G. Castern, K. Hinds, D.W. Grainger, Langmuir 12 (1996) 5083.
[74] X. Gao, Y. Zhang, M.J. Weaver, J. Phys. Chem 96 (1992) 4156.
[75] D.W. Suggs, J.L. Stickney, Surf. Sci. 290 (1993) 375.
[76] D.W. Suggs, J.L. Stickney, J. Phys. Chem. 95 (1991) 10056.